Modeling Chemical EOR Processes: Some Illustrations from Lab to Reservoir Scale

Frédéric Douarche, David Rousseau, Brigitte Bazin, René Tabary, Patrick Moreau, Mikel Morvan

Oil & Gas Science and Technology – Rev. IFP Energies nouvelles

DOI: 10.2516/ogst/2012059

Dossier
Challenges and New Approaches in EOR
Défis et nouvelles approches en EOR

Modeling Chemical EOR Processes: Some Illustrations from Lab to Reservoir Scale

F. Douarche[1]*, D. Rousseau[1], B. Bazin[1], R. Tabary[1], P. Moreau[2] and M. Morvan[2]

1 IFP Energies nouvelles, 1-4 avenue de Bois-Préau, 92852 Rueil-Malmaison Cedex - France
2 Rhodia,178 avenue Schweitzer, 33608 Pessac - France
e-mail: frederic.douarche@ifpen.fr - david.rousseau@ifpen.fr - brigitte.bazin@ifpen.fr - rene.tabary@ifpen.fr - patrick.moreau@eu.rhodia.com - mikel.morvan@eu.rhodia.com

* Corresponding author

Résumé — Modélisation des procédés EOR chimiques : du laboratoire au réservoir — Les procédés de récupération tertiaire par voie chimique, SP (*Surfactant Polymer*) ou ASP (*Alkali-Surfactant-Polymer*), sont en plein essor du fait d'une demande croissante en produits pétroliers. La mise en œuvre des méthodes de récupération d'huile par voie chimique sont très spécifiques et demandent des études intégrées allant de l'étude du réservoir à la simulation du procédé à l'échelle du réservoir, sans oublier les études de laboratoire. Cet article présente le simulateur chimique SARIP^{CH} développé pour les évaluations à l'échelle du réservoir. Il s'agit d'un simulateur de type "*black oil*" incorporant des équations de transport pour les produits chimiques : alcalin, tensio-actif et polymère. Le processus de récupération d'huile est introduit par la courbe de désaturation capillaire. Les réactions physico-chimiques sont décrites en utilisant soit une approche thermodynamique, complète ou simplifiée, soit des tables de façon à rendre les calculs plus efficaces. Dans cet article, on décrit le simulateur et on présente des résultats expérimentaux destinés à valider la physique du simulateur : injection alcaline avec carbonates ou métaborates comme additif alcalin, expériences d'adsorption en fonction de la salinité et du pH, effet systématique de la salinité sur la tension interfaciale et expériences de récupération d'huile avec ou sans gradient de salinité. La bonne adéquation entre résultats expérimentaux et résultats calculés par le simulateur, que ce soit sur les courbes d'élution des produits chimiques ou sur les taux de récupération d'huile, est encourageante et prouve la validité de la physique introduite dans le simulateur. Des études de sensibilité montrent l'impact majeur de la courbe de désaturation capillaire et de l'adsorption sur les taux de récupération d'huile. Pour finir, une approche économique, fondée sur des simulations numériques, fournit des guides à l'échelle du réservoir.

Abstract — Modeling Chemical EOR Processes: Some Illustrations from Lab to Reservoir Scale — *Chemical flooding, SP (Surfactant Polymer) or ASP (Alkali-Surfactant-Polymer), are of increasing interest due to the need to increase oil production. Design of chemical processes is very project specific and requires case by case studies including various steps among which reservoir data analysis, chemical formulations, coreflood validations and reservoir simulation. Every step is dependent on the preceding ones and the last reservoir simulation step gathers all the information collected during the project. In this paper, we present a chemical simulator describing two phase flow with chemical transport of alkali, surfactant, polymer and salinity. Two phase flow is related to capillary desaturation curve through the decrease of oil-water interfacial tension. Physical chemistry reactions are described either with a thermodynamic approach or a simplified one using tables or simplified physics to be compatible with large scale reservoir simulations. In this paper, we describe the simulator and present results of numerous experiments specially designed to validate the model: alkaline injections of carbonates and*

borates, surfactant adsorption experiments at different salinities and pH, systematic effect of salinity on interfacial tension and oil recovery with/without salinity gradient. The good agreement between the experimental and numerical oil recoveries and chemical compositions is very encouraging and supports the validity of the physics implemented in the simulator. In particular, the dominant effect of pH on adsorption and the importance of a salinity gradient on oil recovery is highlighted by numerical simulation. Finally, a sensitivity study at the reservoir scale is presented to illustrate relevant factors for the implementation of an economic surfactant-based process.

INTRODUCTION

Oil mobilization in chemical EOR processes is related to three mechanisms:

- ultra-low interfacial tension for displacement efficiency;
- mobility control for sweep efficiency;
- transport of additives in the formation.

The success of a surfactant flooding SP (Surfactant Polymer), or ASP (Alkali-Surfactant-Polymer) for being general, depends on the simultaneous propagation of a surfactant formulation designed for low interfacial tension, alkaline and polymer at a desired concentration to control oil mobility. The physics is complex and requires to be studied at the laboratory to design the process and to investigate the effect of the main parameters on the oil recovery performance [1]. The simulator, with the appropriate physics, provides an integration of the determinant parameters. It is emphasized as a tool which can be used in very different ways: as an help for the design of experiments to improve the ASP performances and as a tool to scale experiments to pilot and finally to the reservoir scale. The process can be analysed and optimized.

Physics of surfactant processes are well-documented. Efficiency is directly related to InterFacial Tension (IFT) through the capillary number. Low IFT is obtained from phase behavior studies where the salt concentration is a crucial data for the design of the formulation. Since the salinity inside the reservoir during the ASP injection is varying from formation water to injection water or make-up water salinity, formulation work must be done inside a salinity window by looking for a formulation composition giving the lowest IFT when the formation brine mixes with the make-up brine. Numerical simulation can be used to reject surfactant systems which become over-optimized just because the surfactant migrates in the oil-rich phase during flow.

Alkali is added with two targets:

- to reduce surfactant adsorption;
- to generate *in situ* surfactant generally referred as soap [2-4].

Alkali is beneficial for surfactant cost reduction but surfactant needs to be transported behind the alkali front. However, alkali is subjected to losses due to three mechanisms:

- adsorption sometimes referred as hydroxy ion exchange;
- precipitation when alkali is carbonate or metaborate;
- mineral dissolution mainly with the use of caustic at high temperature.

The physics of alkali propagation is well known for carbonates and caustic. Metaborates are promising chemicals, mainly because their tolerance to calcium brines is much higher than carbonates. However, for metaborate the difficulty for modeling the physics leads in the complex chemistry of this additive, with dissociation equilibria involving numerous species. In this paper, we propose a particular physics, based on a pseudo representation to calculate the propagation of metaborate, taking into account the adsorption.

Polymer challenge is mobility control. Addition of polymer into the surfactant slug is still a debate whereas injection of polymer behind the surfactant slug is the rule when reservoir permeability is reasonable. Again, beside experiments, modeling may be used to test the gain in oil recovery obtained by polymer addition into the surfactant formulation.

In this paper, we give a review of IFP Energies nouvelles R&D simulator, which is named SARIP^{CH} (1) [5]. We first describe ASP model capabilities with emphasis on the physics. Then comes a description of laboratory work performed to validate the various options. Alkaline option is validated with caustic, carbonate and metaborate. Ion exchange and precipitation tested at the laboratory are reproduced by the modeling. Finally, the complete validation of oil recovery efficiency is obtained from an experiment performed with a salinity gradient. In a second part, SARIP^{CH} is used to test sensitivity to various parameters affecting the cost of the process, mainly surfactant adsorption or to test the effect of mobility control inside the formulation. Finally, we present results at the pilot scale, in a tridimensional configuration.

1 MODELING OF CHEMICAL EOR PROCESSES

SARIP^{CH} is an in-house two-phase chemical flooding reservoir simulator. Here and below, we assume without any loss of generality that water is the wetting phase and oil is the

(1) The physics of SARIP^{CH} is currently being implemented in the commercial reservoir simulator PumaFlow^{TM} within the OpenFlow^{TM} platform [5].

non-wetting phase and that all the chemical species – polymer, surfactant and alkali – live in the water phase, the oil phase being a dead black oil (no dissolved gas). The flow of this two-phase multi-component system is driven by the generalized Darcy equation, bracketed with each phase mass conservation equation:

$$\begin{aligned} u_i &= -\tfrac{k k_{ri}}{\mu_i}\left(\nabla p_i - \rho_i g\right) \\ \partial_t\left(\rho_i \phi S_i\right) + \nabla\cdot\left(\rho_i u_i\right) &= \delta_i \end{aligned} \tag{1}$$

where the subscript $i = w, o$ labels the water and oil phases, u_i is the Darcy velocity, k is the absolute permeability, k_{ri} is the relative permeability, μ_i is the viscosity, p_i is the pressure, ρ_i is the density, g is the gravity acceleration, ϕ is the porosity, S_i is the saturation such that $\sum S_i = 1$ with $S_w \in [S_{wi}, 1 - S_{or}]$, S_{wi} and S_{or} being the irreducible water and residual oil saturations, and δ_i denotes a source or a sink well term. Specifically, water-phase species mass conservation equations are the following:

$$\begin{aligned} \partial_t M_{wj} + \nabla\cdot\left(\rho_w C_{wj} u_w + j_{wj}\right) &= \delta_{wj} \\ M_{wj} &= \alpha_{wj}\rho_w \phi S_w C_{wj} + \rho_r\left(1-\phi\right) C_{rj} \end{aligned} \tag{2}$$

where C_{wj} is the water-phase j-species concentration (such that $\sum C_{wj} = C_w$), C_{rj} the j-species concentration adsorbed on the rock, α_{wj} the j-species (polymer) volume factor exclusion and j_{wj} the j-species diffusion-dispersion flux. Finally, the closure of the system is ensured with the capillary pressure relationship $p_c(S_w) = p_o(S_w) - p_w(S_w)$.

As we shall see below, because of the surfactant, relative permeabilities are some dynamical functions of the water and oil mobile saturations whose range boundaries S_{wi} and S_{or} may dynamically vary with the capillary number N_c:

$$\begin{aligned} k_{rw}(S_w; N_c) &= f\left[S_w^*(N_c)\right] \\ S_w^*(N_c) &= \tfrac{S_w - S_{wi}(N_c)}{1 - S_{wi}(N_c) - S_{or}(N_c)} \\ k_{ro}(S_w; N_c) &= g\left[S_w^*(N_c)\right] \\ S_o^*(N_c) &= 1 - S_w^*(N_c) \end{aligned} \tag{3}$$

where $S_w \in [S_{wi}(N_c), 1 - S_{or}(N_c)]$ and $S_w^* \in [0, 1]$. For example, relative permeabilities can follow Corey power laws, that is:

$$\begin{aligned} k_{rw}(S_w; N_c) &= k_{rw}^0 (S_w^*)^{n_w} \\ k_{ro}(S_w; N_c) &= k_{ro}^0 (1 - S_w^*)^{n_o} \end{aligned} \tag{4}$$

the k_{ri}^0 and n_i being possibly some functions of N_c. However, in most cases relative permeabilities will belong to some family of numerical tables indexed by the capillary number; the same holds for the capillary pressure (*e.g.*, $p_c(S_w^*) = p_e/(S_w^*)^{\frac{1}{\lambda}}$ where p_e is the displacement pressure and λ some exponent [6]), since the irreducible water and residual oil saturations dynamically depend on the capillary number:

$$\begin{aligned} k_{ri}(S_w; N_c) &= k_{ri}[S_w; S_{wi}(N_c), S_{or}(N_c)] \\ p_c(S_w; N_c) &= p_c[S_w; S_{wi}(N_c), S_{or}(N_c)] \end{aligned} \tag{5}$$

Some authors defined the capillary number N_c as the dimensionless ratio of the water phase driving viscous force over the oil-water IFT, that is $N_c = \mu_w u_w/\sigma_{ow}$, where σ_{ow} is the oil-water IFT [7-11]. However, several definitions are possible as long as they are relevant and consistent [11-14]; in SARIP$^{\text{CH}}$, we chose $N_c = (R_m \mu_w u_w + \mu_o u_o)/\sigma_{ow}$ where R_m is the polymer mobility reduction.

The Capillary Desaturation Curve (CDC) relationship, $S_{or} = S_{or}(N_c)$, relates the residual oil saturation as a function of the capillary number [9]. The lower the IFT is, the lower the residual oil saturation is, the higher the 'free' recoverable oil is and the higher the capillary number is. However, in order to be truly effective, the surfactant has to lower the IFT over several orders of magnitude, say from $\sigma_{ow} = 30$ mN/m without any surfactive agent to 10^{-4} mN/m with an efficient and cost-effective surfactant (see *Fig. 3b*), hence the logarithmic scale in N_c as shown in Figure 3a. Indeed, the increase of N_c over several orders of magnitude results in a significant residual oil saturation reduction.

Clearly, the oil-water IFT σ_{ow} is a function of the surfactant concentration. More critically, it is above all a critical function of the water salinity (or Total Dissolved Solids (TDS) in water concentration), as can be seen in Figure 3b [15, 16]. Indeed, for one given surfactant concentration, the IFT exhibits a critical ultra-low minimum at the optimum salinity S^* and a logarithmic increase over several orders of magnitude in the vicinity of S^*. Therefore, the IFT $\sigma_{ow} = \sigma_{ow}(C_{ws}, S, \{C_{wa}\})$ dynamically depends on the surfactant concentration C_{ws}, on the salinity S, and on the alkali concentration(s) $\{C_{wa}\}$ if any. It should be noted that despite the modeling is two-phase, the IFT encompasses the full Winsor surfactant three-phase critical behavior in an effective and simple manner.

Alkali, polymer and surfactant species adsorptions are Langmuir-like [17, 18]. More sophisticated is the case of the surfactant, where the Langmuir plateau is a product function of the water salinity (say chloride and sodium ions concentrations) and pH (say hydroxide ions concentration), in order to take into account the alkali effect on limiting the surfactant adsorption:

$$\begin{aligned} C_{rj} &= C_{rj}^0 \frac{K_j C_{wj}}{1 + K_j C_{wj}} \qquad j = s, p, \{a\} \\ C_{rs}^0 &= \text{linear function of (salinity, pH)} \end{aligned} \tag{6}$$

where C_{rj}^0 is the maximum j-species concentration adsorbed on the rock (Langmuir plateau) and $K_j(T)$ is the j-species equilibrium constant at temperature T.

Additional features are alkali-rock reactions through ion exchange and dissolution-precipitation. Ion exchange reactions involving calcium, magnesium, potassium and sodium cations are written below [19]. Ion exchange equilibrium constants and solubility products used in the simulation

were close to equilibrium constants found in the litterature (see *Tab. 1*):

$$\begin{aligned}
\frac{C_{r\mathrm{Ca}^{2+}}}{C^2_{r\mathrm{Na}^{+}}}\frac{C^2_{w\mathrm{Na}^{+}}}{C_{w\mathrm{Ca}^{2+}}} &= \frac{K_{21}}{Q_0} = K'_{21}\\
\frac{C_{r\mathrm{Ca}^{2+}}}{C^2_{r\mathrm{K}^{+}}}\frac{C^2_{w\mathrm{K}^{+}}}{C_{w\mathrm{Ca}^{2+}}} &= \frac{K_{25}}{Q_0} = K'_{25}\\
\frac{C_{r\mathrm{Mg}^{2+}}}{C^2_{r\mathrm{Na}^{+}}}\frac{C^2_{w\mathrm{Na}^{+}}}{C_{w\mathrm{Mg}^{2+}}} &= \frac{K_{61}}{Q_0} = K'_{61}\\
C_{w\mathrm{Ca}^{2+}}C_{w\mathrm{CO}_3^{2-}} &= K_{s2}\\
C_{w\mathrm{Mg}^{2+}}C_{w\mathrm{CO}_3^{2-}} &= K_{s6}
\end{aligned} \tag{7}$$

TABLE 1

Ion exchanges equilibrium constants and solubility products (see the text)

K_1	2×10^{-8} mol/L	K_{21}, K_{61}	3.9 mol/L
K_2	1.2×10^{-4} mol/L	K_{25}	0.2 mol/L
K_3	10^{-14} (mol/L)^2	Q_0	0.077 mol/L solid
K_{s2}	2×10^{-8} (mol/L)^2	$Q_{\max}$	0.03 mol/L solid
K_{s6}	1.5×10^{-4} (mol/L)^2	K_e	30 000 L/mol

2 ION EXCHANGE IN THE CONTEXT OF A HIGH SALINITY PREFLUSH

This simulation addresses a realistic strategy of surfactant injection in a context of high divalent cation concentration. Preflush injection can be recommended when surfactants with limited tolerance to divalent cations are used. Injection of high salinity brine is a way to decrease divalent cation concentration ahead of the surfactant slug owing to ion exchange mechanisms.

In the initial situation, the core is equilibrated with reservoir water, clays are saturated with the four cations (*Tab. 2*). Ion exchange capacity of the reservoir sandstone is 7.2 meq/100 g (*Tab. 1*). This high cation exchange capacity is related to a high clay content, which is mainly made of smectites. When potassium chloride is injected, calcium, magnesium and sodium cations are replaced by potassium. Figure 1 shows the comparison of simulation

TABLE 2

Composition of reservoir water for preflush validation in SARIP^{CH}

Ion	Concentration (ppm)
Na^+	576
Ca^{2+}	96
Mg^{2+}	46
K^+	0
Cl^-	1 193
CO_3^{2-}	0

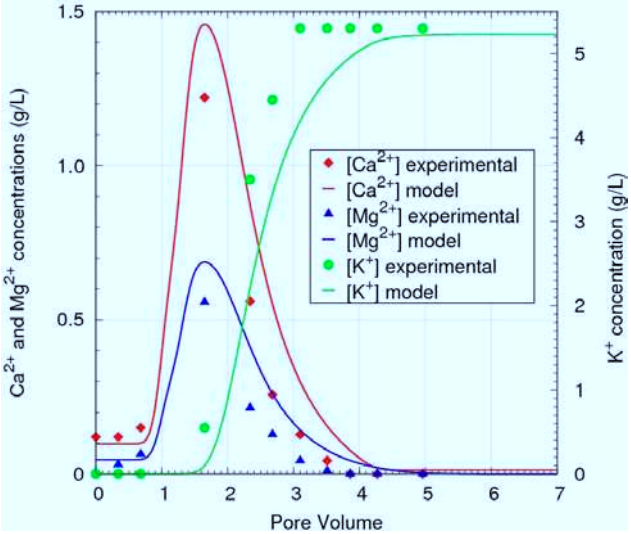

Figure 1

Comparison of ions exchange simulation and experimental results.

and experimental results. Release of calcium and magnesium occurred at one injected Pore Volume (PV) according to the chromatographic theory for ion exchange. A very large preflush size is necessary if a complete release of divalent cations is required. Addition of alkaline additive is a way to shorten the cation release.

3 ALKALI TRANSPORT: THE 'PSEUDO-OH' MODEL FOR SIMPLIFIED PH CALCULATION

In the case of alkali transport, the pH (*i.e.* the concentration in OH^- ions) of the water phase in the zones of the reservoir contacted with the alkali-surfactant slug is a key parameter. Indeed, its determination is needed to predict the amount of alkali to be injected to achieve a satisfactorily reduction of surfactant adsorption, which directly impacts the oil recovery. The pH is controlled by the chemical equilibria associated to the injected alkaline agent and by the adsorption of OH^- ions on the rock surface. For the simulation, it is useful to consider separately the case when the alkali is caustic soda (NaOH) and the general case of an alkali being a base which leads to a buffer effect.

Case #1: if the alkali is NaOH, transport of the OH^- ions and hence pH can be rather straightforwardly determined, provided the Langmuir isotherm adsorption parameters (*Eq. 6*) for the OH^- ions are known.

Case #2: if the alkali is a more complex base, the OH^- concentration is controlled both by OH^- adsorption and by the relevant chemical equilibria corresponding to the base used. As a consequence, pH determination requires solving a system of equations in each grid block. This

TABLE 3

Core properties and main experimental parameters for the reference monophasic coreflood injections of sodium carbonate (Na_2CO_3) and sodium tetraborate

Alkali agent injected	Na_2CO_3	Sodium tetraborate
Porous medium	Synthetic granular pack with 95 wt% silica and 5 wt% kaolinite	Synthetic granular pack with 95 wt% silica and 5 wt% kaolinite
Diameter	2 cm	2 cm
Length	7 cm	7 cm
Porosity	25%	25%
Brine initially in place	NaCl 10 g/L	NaCl 10 g/L
Alkali concentration in the injection slug	10 g/L	10 g/L
NaCl concentration in the injection slug	10 g/L	10 g/L
pH of the injection slug	11.4	9.5
Volume of the injection slug	1 PV	1 PV
Volume of 10 g/L NaCl chase water injected	6.5 PV	7 PV
Darcy velocity	80 cm/d	80 cm/d
Temperature	40°C	Ambient

method is described in particular in [20] for carbonate (reaction 5) and in [21] (reactions 3 and 4) for metaborate. As will be shown with the first example below, it gives satisfactorily results when compared to experimental data. However, the corresponding computation times can be significantly long. In addition, such full calculations require to input the chemical equilibrium thermodynamic constants, which are not always well known, for example in the case of metaborate. This method can thus potentially lead to erroneous pH calculation and/or entail over-lengthy simulations. Furthermore, in the case of some complex base (like tetraborate), the relevant chemical equilibria involved may not be known, rending the simulation impossible. For these reasons, a complete calculation method is not always practically applicable.

The 'pseudo-OH' model is an alternative to the complete calculation method for the injection of bases which are not NaOH. It relies on a simplified (but practically relevant) determination of the pH in each grid block which assumes that, instead of the actual alkaline agent, only pseudo OH^- ions with specific adsorption parameters are transported in the porous medium. Determination of these parameters is achieved through a fit of the effluent pH results of a reference monophasic alkali-injection coreflood. The whole process for simulating a given reservoir case hence involves 3 steps:

a) reference monophasic coreflood experiment on a rock sample representative of the reservoir under study: injection of the actual alkaline agent to be used in the case, measurement of the injected solution pH and of the pH in the effluents (called effluent pH in the following);
b) simulation of this experiment with the NaOH model (case #1) with an injected OH^- concentration corresponding to the pH of the actual solution injected in the experiment. Several simulations are performed to fit the effluent pH experimental data, by adjusting the adsorption parameters C_r^0 and K (*Eq. 6*) for the adsorption of the 'pseudo-OH' ions;
c) simulation of the full-scale reservoir case, the alkali transport being computed with the NaOH model, with, for the 'pseudo-OH' ions, a concentration being the concentration corresponding to the pH of the actual alkaline agent solution and the adsorption parameters being the parameters determined in step b).

4 IMPLEMENTATION OF THE 'PSEUDO-OH' MODEL

In this section, we present two examples of the implementation tests of steps a) and b) of the 'pseudo-OH' model.

4.1 Example 1: Sodium Carbonate (Na_2CO_3) Injection

The experimental conditions are detailed in Table 3. The core (a synthetic granular pack made of 95 wt% silica and 5 wt% kaolinite) is initially saturated with 10 g/L NaCl brine. A volume of 5.5 mL (corresponding to 1 PV) of 10 g/L Na_2CO_3 solution in the same 10 g/L NaCl brine is then injected. After the alkali injection, 35.7 mL (6.5 PV) of 10 g/L brine is then injected as chase water. The pH of the alkaline solution is 11.4. The concentration of OH^- ions can be determined graphically from plots such as those presented in Figure 2a, analytically from the resolution of the chemical equilibria involved with Na_2CO_3 or directly from the pH of the injected alkaline solution. For the present experiment, the injection concentration of OH^- ions to be used for the 'pseudo-OH' model is $[OH^-] = 0.092$ g/L. In the numerical simulations, the same injection sequences as in the experiment are performed. The alkali slug in particular must have the same size as in the experiment (1 PV).

In Figure 2b are presented the experimental effluent pH data (dots) and the 'pseudo-OH' numerical results

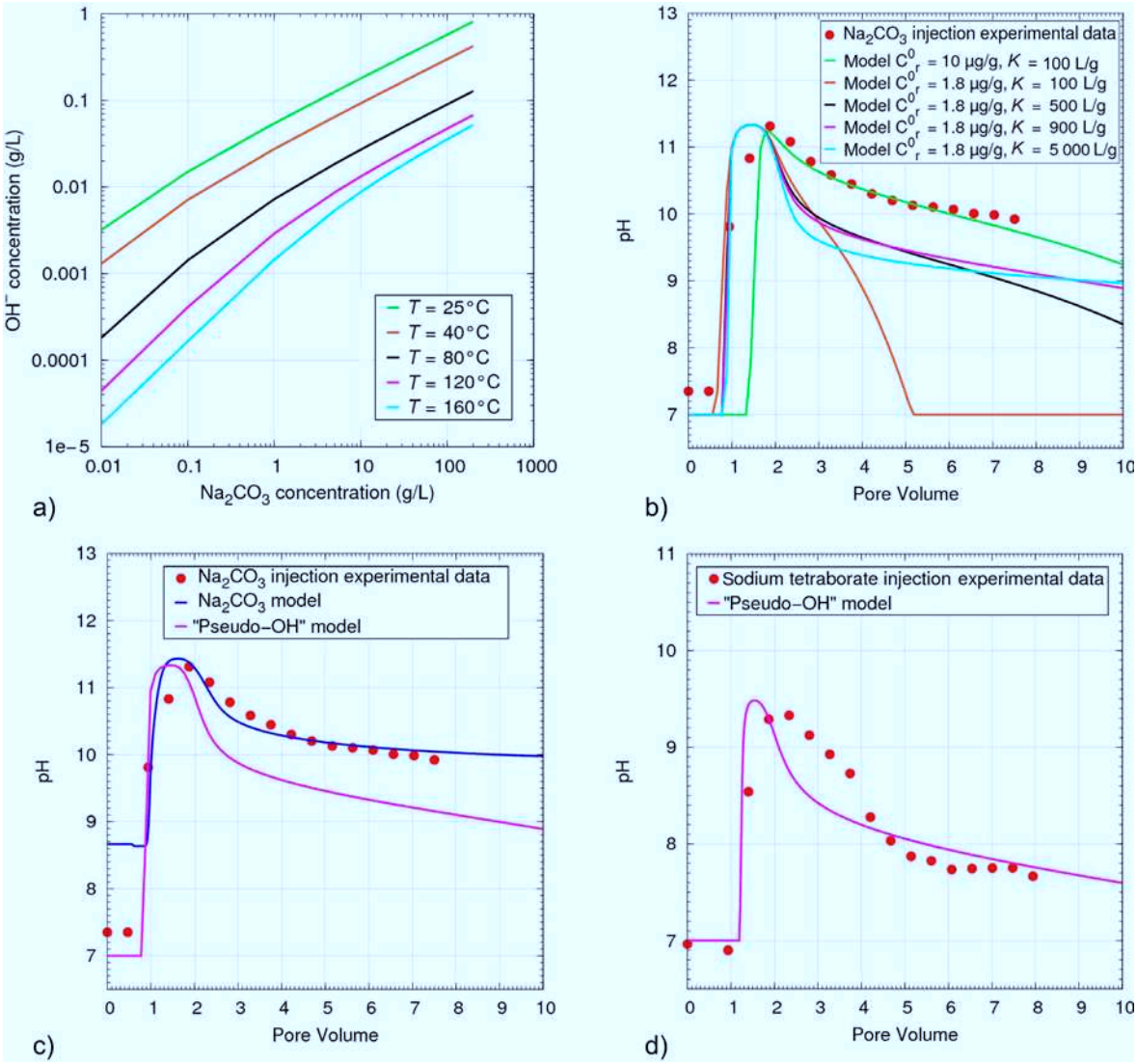

Figure 2

a) Graphical illustration of the determination of the equivalent concentration in OH^- as a function of Na_2CO_3 concentration and temperature. b) Na_2CO_3 injection, determination of the C_r^0 and K parameters of the 'pseudo-OH' ions by adjustment of effluent pH experimental data. The 'pseudo-OH' concentration used is $[OH^-]$ = 0.092 g/L. The best fit is obtained for C_r^0 = 1.8 µg/g and K = 900 L/g. c) Na_2CO_3 injection, effluent pH. Comparison between the Na_2CO_3 model, the 'pseudo-OH' model and the experimental data. 'Pseudo-OH' model parameters are: $[OH^-]$ = 0.092 g/L, C_r^0 = 1.8 µg/g and K = 900 L/g. Both the Na_2CO_3 and the 'pseudo-OH' model satisfactorily predicts the breakthrough and the maximum pH value. d) Sodium tetraborate injection, effluent pH. Comparison between the 'pseudo-OH' model and the experimental data. 'Pseudo-OH' model best-fit parameters are: $[OH^-]$ = 0.0014 g/L, C_r^0 = 0.075 µg/g and K = 30 000 L/g. The 'pseudo-OH' model satisfactorily predicts the breakthrough and the maximum pH value.

(curves) *versus* the total volume of liquid injected (normalized in PV). To illustrate the adjustment procedure implemented, several curves are shown, each of them corresponding to the result of a simulation run performed with a given pair of C_r^0 and K values. The criterion for best fit here is qualitative: correct representation of the pH breakthrough and of the pH maximum value are privileged rather than least-squares minimization. This approach is justified by the fact that reservoir-scale simulations involve alkali-surfactant slug always lower than 1 PV and chase water slug volumes of 1 PV maximum. For this experiment, the best fit is obtained with C_r^0 = 1.8 µg/g and K = 900 L/g. For this simulation, and for all simulations resulting in a correct adjustment of the pH breakthrough, it appears that the simulated pH decreases faster than the measured pH. This is due to the lack of buffer effect when directly injecting OH^-.

Figure 2c shows a comparison between simulations of the experiment with the 'pseudo-OH' model and a model involving the complete calculation of the carbonate acid-base equilibria (Na_2CO_3 model). It appears that,

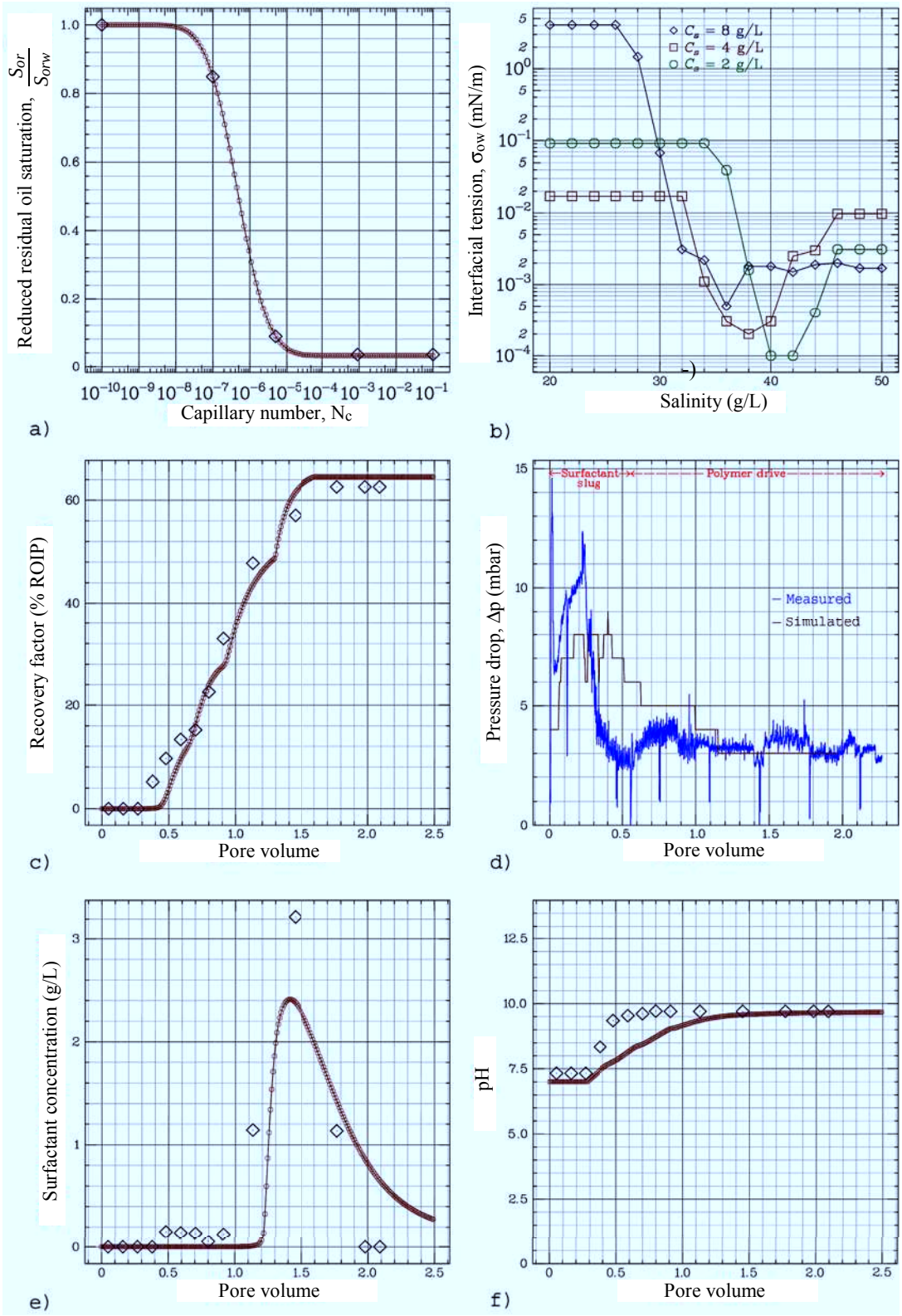

Figure 3

Coreflood measurements and simulation results comparison. a) Measured capillary desaturation curve (blue symbols), b) measured IFT as a function of salinity for several surfactant concentrations, c) recovery factor (ROIP stands for residual oil in place, blue symbols are experimental measurements and red continous lines are simulation outputs), d) pressure drop, e) surfactant concentration in the effluent, f) produced water pH.

disregarding the pH value before the breakthrough (discrepancies are due to different model initializations), the two simulations satisfactorily reproduce the experimental results up to about 2 PV, which is largely sufficient for the simulation of real field cases.

4.2 Example 2: Sodium Tetraborate Injection

For the injection of complex alkaline agents or of alkali slugs with several species, using a 'pseudo-OH' model can be the only way to perform a simulation. The example experiment presented in this paper consists in the injection of a sodium tetraborate solution at 10 g/L concentration, with a pH of 9.5. The other conditions of this experiment, reported in Table 3, are comparable to those for the Na_2CO_3 injection. For this experiment, the injection concentration of OH^- ions in the 'pseudo-OH' simulations is determined from the measurement of the pH of the injected solution, namely $[OH^-] = 0.0014$ g/L. However, to generalize the method and speed-up the process, standard curves linking alkali concentration and pH or OH^- concentration could be built. In the numerical simulations, again, the same injection sequences as in the experiment are performed and the alkali slug must have the same size as in the experiment (1 PV).

In Figure 2d are presented the experimental effluent pH data (dots) and the best-fit 'pseudo-OH' numerical results (curve) *versus* the total volume of liquid injected (normalized in PV). This best fit was obtained with $C_r^0 = 0.075$ μg/g and $K = 30\,000$ L/g. The figure shows that, similarly as with the Na_2CO_3 injection, the pH breakthrough and the maximum pH value are satisfactorily reproduced by the 'pseudo-OH' model. It also appears that the discrepancy between the simulated and the experimental pH during long-term chase water injection is less marked than with Na_2CO_3. This originates in the fact that, due to the lower pH value obtained, the model is less sensible to the absence of buffer effect with OH^- injection.

5 ASP SALINITY GRADIENT COREFLOOD

Results presented below illustrate an ASP salinity gradient process to maximize oil recovery. Surfactant phase behavior, surfactant adsorption and polymer viscosity data were obtained from a parallel study reported in a companion paper [1]. Experiments with synthetic representative crude, reservoir formation brine and surfactant solutions were performed to determine the optimum solubilization ratio and optimum salinity, as well as to screen surfactants and polymer for compatibility. Based on the laboratory measurements, the optimum IFT is about 5×10^{-4} mN/m using the Huh relation ([22]; see *Fig. 3b*). The polymer selected by laboratory testing was a hydrolyzed polyacrylamide (*SNF* Flopaam 3330S). The injection flow rate is 3 cm^3/h. The properties of this coreflood are summarized in Table 4 and include porosity, permeability, fluid volumes and relative permeabilities.

The salinity is continuously decreased from 50 g/L in the waterflooding water up to 25 g/L in the chase water (see *Tab. 5*). The surfactant slug is 0.55 PV at a surfactant concentration of 8 g/L in 30 g/L NaCl and 10 g/L Na_2CO_3. The surfactant slug is in a Winsor I type. The polymer drive is at a salinity of 25 g/L NaCl + 10 g/L Na_2CO_3. The optimal salinity is at 36 g/L NaCl + 10 g/L Na_2CO_3. The schedule of this coreflood and its pseudo companion are summarized in Tables 5 and 6.

Coreflood measurements and simulation results are summarized in Figures 3c-f. Surfactant concentration has been determined by Hyamine titration. It must be emphasized that a mass balance on surfactant effluents shows retention of 160 μg/g of rock. The simulated oil bank breakthrough (see *Fig. 3c*), which occurs at 0.4 PV, is in good agreement with the measured one, which occurs around 0.3 PV, the recovery factor slope and amplitude being in excellent agreement. The surfactant breakthrough shown in Figure 3e is also well reproduced within a 10% error. The simulated pressure drop reported in Figure 3d reasonably fits the measured one; they both share the well known one-dimensional constant flow rate waterflooding behavior [23]. Finally, as reported in Figure 3f, the pH amplitude and its PV threshold are well reproduced, apart a noticeable time lag regarding the reach of the final plateau value.

6 QUARTER 5-SPOT CHEMICAL DISPLACEMENT SENSITIVITY ANALYSIS

The goal of this section is to give by a reservoir simulation sensitivity analysis, realistic tertiary SP flood recovery factor estimated on the basis of a tridimensional vertically heterogeneous quarter 5-spot 'toy model' (taken from a previous study), and to show how the tertiary oil recovery performance may depend on surfactant adsorption, surfactant concentration, surfactant slug size, CDC, and eventually how a pre-existent secondary waterflood of variable duration may affect the tertiary recovery factor.

The reservoir investigated in this study is 924 m deep and 13 m thick. The reservoir is currently undergoing waterflood and is producing about 98% water-cut, which is close to the economic limit. The properties of this reservoir are summarized in Table 7 and include porosity, permeability, fluid volumes and relative permeabilities. The residual saturations, relative permeability end points and relative permeability Corey exponents were derived from laboratory data and are typical of a water-wet reservoir. In addition, the reservoir fluid properties were also obtained from the field operator and are listed in Table 7.

The simulation model is a quarter five-spot symmetry element with a pressure-constrained injector and producer

TABLE 4

Coreflood and simulation model properties

Geometry	
Core length	$L = 9.78 \times 10^{-2}$ m
Core diameter	$D = 4.92 \times 10^{-2}$ m
Core cross sectional area	$A = 1.9 \times 10^{-3}$ m^2
Volumetrics	
Irreducible (connate) water saturation	$S_{wi} = 0.253$
Residual oil saturation (waterflooding)	$S_{orw} = 0.568$
Residual oil saturation (chemical flooding)	$S_{orc} = 0.018$
Porosity	$\phi = 0.159$
Porous volume	$V_p = 2.9564 \times 10^{-5}$ m^3
Residual oil in place	ROIP $= 1.6792 \times 10^{-5}$ m^3
Polymer properties	
Mobility reduction	$R_m = 1.8$
Core conditions	
Core temperature	$T_c = 60°$C
Core pressure	$p_c = 2$ bar
Flow properties	
Water density at core conditions	$\rho_w(T_c, p_c) = 983.28 \times 10^{-3}$ kg/m^3
Oil density at core conditions	$\rho_o(T_c, p_c) = 719.95 \times 10^{-3}$ kg/m^3
Water viscosity at core conditions	$\mu_w(T_c, p_c) = 0.46642$ cP
Oil viscosity at core conditions	$\mu_o(T_c, p_c) = 0.80123$ cP
Horizontal absolute permeability	$k = 850$ mD
Maximum water relative permeability (waterflooding)	$k_{rw}(1 - S_{orw}) = 0.580$
Maximum water relative permeability (chemical flooding)	$k_{rw}(1 - S_{orc}) = 0.048$
Maximum oil relative permeability (waterflooding)	$k_{ro}(S_{wi}) = 0.690$
Maximum oil relative permeability (chemical flooding)	$k_{ro}(S_{wi}) = 0.690$
Water relative permeability Corey exponent (water- & chemical-flooding)	$n_w = 2$
Oil relative permeability Corey exponent (water- & chemical-flooding)	$n_o = 2$
Flow rate	
Water phase injection rate	$Q_{\text{inj}} = 3$ cm^3/h $= 7.2 \times 10^{-5}$ m^3/d
Water & oil phases total production rate	$Q_{\text{prod}} = Q_{\text{inj}}$

TABLE 5

ASP coreflood injection schedule

	Water (PV)	NaCl (g/L)	Na_2CO_3 (g/L)	Surfactant (g/L)	Polymer (ppm)
Water in place	–	50	–	–	–
Surfactant slug	0.55	30	10	8	0
Polymer slug	1.72	25	10	0	750
Flush water	2.52	25	10	0	0

TABLE 6

ASP coreflood pseudo injection schedule. The Langmuir hydroxide ions adsorption is such that $C^0_{r\text{OH}^-} = 0.12$ µg/g and $K_{\text{OH}^-} = 900$ L/g

	Water (PV)	NaCl (g/L)	NaOH (g/L)	
Surfactant slug	0.55	30	4.7×10^{-3}	
Polymer slug	1.72	25	4.7×10^{-3}	
Flush water	2.52	25	4.7×10^{-3}	
	Water (PV)	Na^+ (g/L)	Cl^- (g/L)	OH^- (g/L)
Surfactant slug	0.55	11.81	18.20	2×10^{-3}
Polymer slug	1.72	9.84	15.16	2×10^{-3}
Flush water	2.52	9.84	15.16	2×10^{-3}

TABLE 7

Reservoir and simulation model properties

Geometry	
Reservoir thickness (single z layer)	$H = 13$ m
Reservoir layers thickness (layer cake, from top to bottom)	$H_1 = 4.75$ m
	$H_2 = 3.00$ m
	$H_3 = 5.25$ m
Reservoir x-y linear extension	$L = 267.75$ m
Reservoir top depth	$z_{\text{top}} = 924$ m
Volumetrics	
Irreducible water saturation	$S_{wi} = 0.35$
Residual oil saturation (waterflooding)	$S_{orw} = 0.32$
Residual oil saturation (chemical flooding)	$S_{orc} = 0.016$
Porosity	$\phi = 0.25$
Porous volume	$V_p = 232\,999.47$ m^3
Original Oil In Place (at reservoir conditions)	OOIP = 151 454.04 m^3
Residual Oil In Place (at reservoir conditions)	ROIP = 74 561.99 m^3
Reservoir conditions	
Reservoir temperature	$T_{\text{res}} = 53°$C
Reservoir pressure	$p_{\text{res}} = 40$ bar
Polymer properties	
Mobility reduction	$R_m = 5$
Flow properties	
Water viscosity at reservoir conditions	$\mu_w(T_{\text{res}}, p_{\text{res}}) = 0.55$ cP
Oil viscosity at reservoir conditions	$\mu_o(T_{\text{res}}, p_{\text{res}}) = 12$ cP
Horizontal x-y absolute permeability (1st layer)	$k_h^{(1)} = 100$ mD
Horizontal x-y absolute permeability (2nd layer)	$k_h^{(2)} = 50$ mD
Horizontal x-y absolute permeability (3rd layer)	$k_h^{(3)} = 500$ mD
Horizontal-vertical permeability coupling	$k_v/k_h = 0.1$
Maximum water relative permeability	$k_{rw}(1 - S_{orw}) = 0.1$
Maximum oil relative permeability	$k_{ro}(S_{wi}) = 1$
Water relative permeability Corey exponent (water- & chemical-flooding)	$n_w = 1.6487$
Oil relative permeability Corey exponent (water- & chemical-flooding)	$n_o = 4.9628$
Wells	
Injection and production well radius (perforation on all layers)	$r_w = 7$ cm
Water phase injection rate ($\frac{1}{4}$ 5-spot)	$Q_{\text{inj}} = 37.5$ m^3/d
Water and oil phases total production rate	$Q_{\text{prod}} = Q_{\text{inj}}$
Maximum bottom-hole injection pressure	$p_{\text{inj}} = 150$ bar
Minimum bottom-hole production pressure	$p_{\text{prod}} = 15$ bar

within a 2.8676×10^5 m^2 pattern (70 acre). Well test measurements indicated that the reservoir can be described as layered with one bottom high permeability layer stacked with two lower permeability layers (see *Tab. 7*). Due to the lack of any other available operator data, we assumed the planar permeability field to be homogeneous in each layer.

The reservoir has had a very long history of primary and secondary recovery. We did not try to obtain a realistic post-waterflood oil saturation and pressure distribution; rather, we adopted a very phenomenological two-fold approach: first, we crudly assumed that all the oil that could be displaced by waterflooding had been produced, that is to say we did not simulate nor match the waterflood and started from scratch the tertiary chemical injection from a 'perfect' tertiary initial state (*i.e.* $S_w(x, t = 0^-) = 1 - S_{orw}$ at any point x of the reservoir). This case is probably highly unrealistic but is also the most unfavorable scenario regarding the chemical injection, since there is no remaining 'free' oil in the reservoir that could be ultimately produced by waterflooding and that could be eventually produced by the chemical injection. In a second approach, a waterflood of variable duration was simulated with known well constraints and ceased at several realistic water-cuts; in this case, the simulated post-waterflood conditions were used as the initial conditions for all SP simulations.

Surfactant phase behavior, surfactant adsorption and polymer mobility reduction were obtained from a previous study. Experiments with reservoir crude and formation brine, and surfactant solutions were performed to determine the optimum salinity and solubilization ratio, as well

TABLE 8

Quarter 5-spot base case tertiary SP injection schedule (surfactant adsorption is 200 μg/g)

	Water (PV)	Surfactant (g/L)	Polymer (ppm)
Surfactant slug	0.3	10	500
Polymer slug	1.7	0	1 000

as to screen surfactants and polymer for compatibility. Based on the laboratory data, the optimum IFT is about 3.6×10^{-3} mN/m using the Huh relation [22]. In addition, experimental corefloods were conducted to measure the performance of the surfactant and polymer. In particular, the surfactant adsorption was measured in several corefloods and ranged from 100 to 400 μg/g with an average value of 200 μg/g. Measurements also shown that polymer adsorption could be neglected.

The base case simulation was designed by utilizing known field conditions and laboratory coreflood designs. The known field conditions included a maximum bottom-hole injection pressure of 150 bar and a minimum bottom-hole production pressure of 15 bar. The injection well constraint is due to the reservoir fracture pressure and the producer constraint is due to facility constraints from the field of interest. The laboratory coreflood designs were used to develop the base case injection scheme for the chemical flood. The SP design for the base case simulation is summarized in Table 8: a 0.3 PV surfactant with polymer slug is followed by a 1.7 PV polymer drive slug; of course, thumb's rule for the polymer drive slug size is rather 0.5 PV but here, our phenomenological goal is only to give rough recovery estimates and relative variations on a 'large' time scale.

Figure 4 reports the tertiary recovery factor sensitivity to surfactant adsorption (*Fig. 4a, b*), surfactant concentration (*Fig. 4c, d*), and surfactant slug size (*Fig. 4e, f,* in that case, the polymer drive slug varies accordingly to the surfactant slug size so that the total injection duration is 2 PV), reminding that the base case surfactant adsorption is 200 μg/g, surfactant concentration is 10 g/L and surfactant slug size is 0.3 PV. The base case CDC (Capillary Desaturation Curve) is shown in Figures 5a and d.

As shown in Figure 4b, where each curve is a snapshot at some time (injected PV) for several surfactant adsorptions ranging from 0 to 900 μg/g, the recovery factor decreases quasi-linearly in the surfactant adsorption. This is an important trend due to its non saturating feature, contrary to an asymptotic logarithmic variation, *e.g.*, as we shall see below. Base case final recovery factor is 20% ROIP (ROIP stands for Residual Oil In Place); 2% additional ROIP can be gained if the surfactant is assumed not to adsorb on the rock, which is unlikely. On the other hand, the more pessimistic 400 μg/g surfactant adsorption leads to a 16% ROIP final recovery factor. A noticeable gap of about 3% ROIP appears in the oil recovery between the 400 and the 300 μg/g surfactant adsorption cases.

Figures 4c, d report the recovery factor sensitivity to the surfactant concentration, ranging from 2 to 40 g/L, 10 g/L being the base case and leading to a 20% ROIP recovery factor. In that case, the recovery factor increases non-linearly with the surfactant concentration; there is a noticeable change in the recovery factor — almost 4% ROIP — if the surfactant concentration is increased from 10 to 15 g/L. Of course, higher surfactant concentrations lead to better recoveries but since the recovery process is non-linear in the surfactant concentration, the additional recovered oil is not proportional to the increase of the surfactant concentration. Besides, large time scale injection also seems to play a key role: indeed, the recovery factor exhibits a large gap between 0.75 and 1 injected PV, after what the recovery factors amplitudes are translated from each other, which is not the case below 1 injected PV.

Finally, Figures 4e, f report the recovery factor sensitivity to the surfactant slug size, ranging from 0.1 to 1 injected PV, 0.3 injected PV being the base case and leading to a 20% ROIP recovery factor. This case exhibits a strong non-linear dependence of the recovery factor in the surfactant slug size, with a large gap between 0.2 and 0.3 injected PV (4% ROIP). This gap is by far larger between 0.1 and 0.2 injected PV (8-9% ROIP).

The last part of this sensitivity study is dedicated to the tertiary recovery factor dependence in the CDC and in a pre-existent waterflood of variable duration. We start with the CDC (see *Fig. 5a-c*), the tertiary reservoir initial conditions and injection schedule being the same as the ones which have been previously used and reported in Table 8. The base case CDC is shown in Figure 5a (red symbols are measured CDC while its fitting companion curve is continuous line, curve [1] in the figure). We first translate this base CDC without modifying its shape (nor the independent IFT table) to lower capillary number values twice half an order of magnitude successively, which leads to CDCs [2] and [3]. Secondly, the base CDC slope is increased, which leads to CDC [4], then shifted half an order of magnitude to the left (CDC [5]) and finally one more order of magnitude to the left (CDC [6]). Corresponding recovery factors in % ROIP and % OOIP (OOIP stands for Original Oil In Place) are reported in Figures 5b, c: comparison between recovery factors [1] and [3] shows that a one order of magnitude N_c-shift of the CDC results in a doubling of the recovery factor in % ROIP or % OOIP. Comparison between recovery factors [2] and [6], and [1] and [2] approximately gives the same estimate; in the latter case, half an order of magnitude

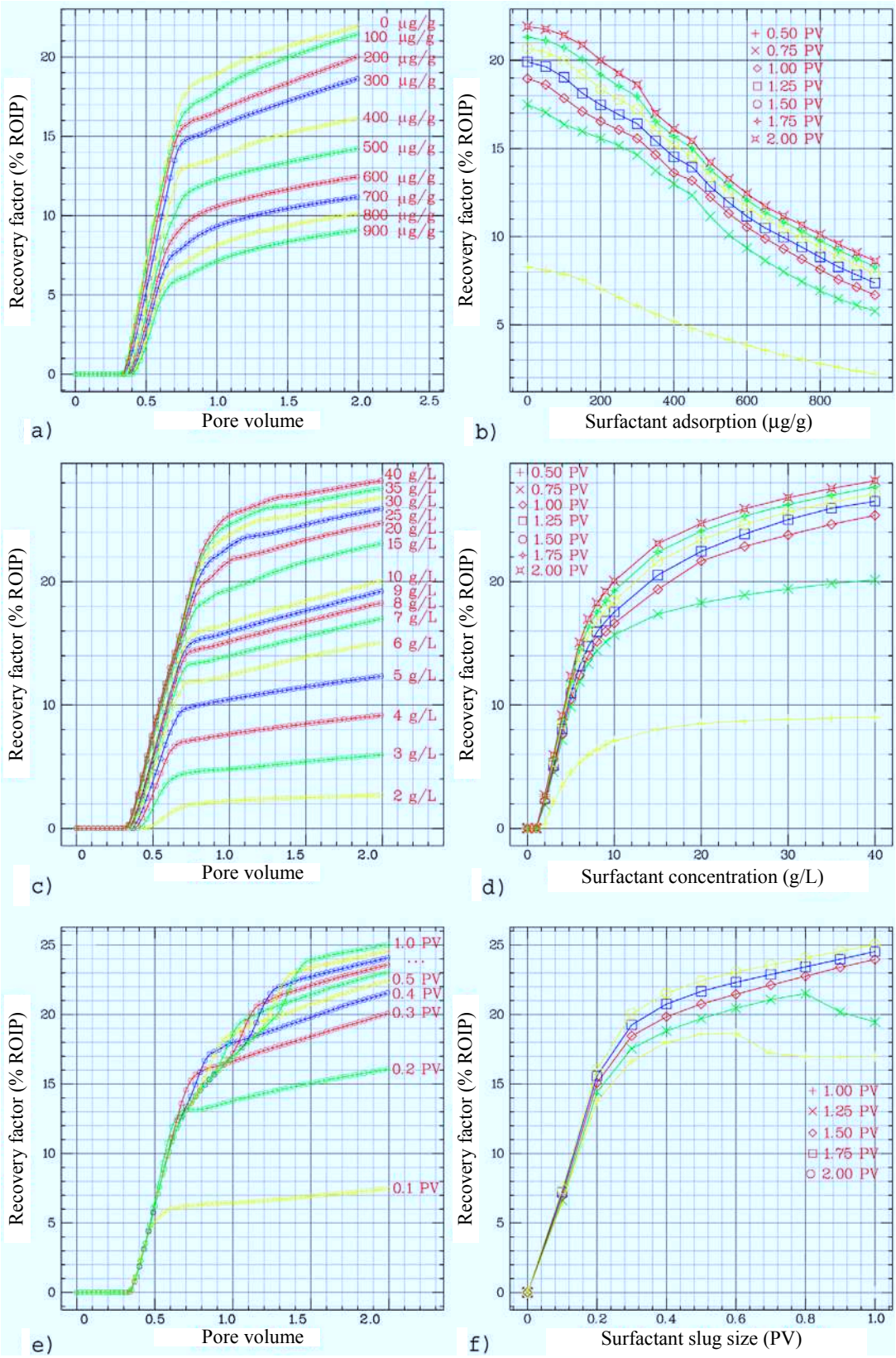

Figure 4

Quarter 5-spot tertiary recovery factor sensitivity study to a,b) surfactant adsorption, c,d) surfactant concentration and e,f) surfactant slug size.

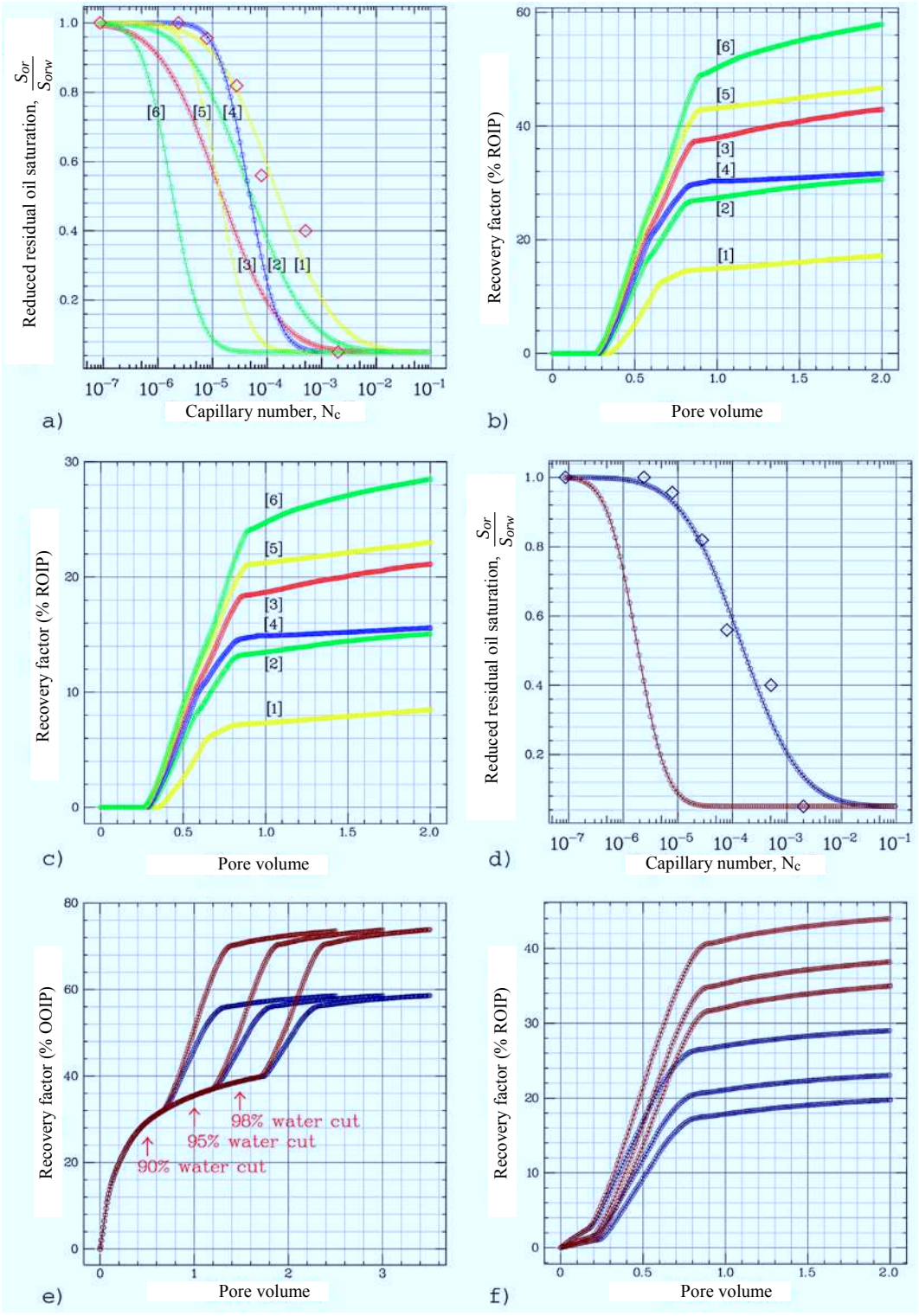

Figure 5

Quarter 5-spot recovery factor sensitivity study to: capillary desaturation curve (CDC) in stricly tertiary conditions [a-c); waterflood is assumed to be of infinite duration and has not been simulated]; a pre-existent waterflood of finite variable duration d-f), considering the most favorable and defavorable CDCs [1] and [6] (ROIP stands for Residual Oil In Place and OOIP stands for Original Oil In Place). The references for the curve numbers are described in the text.

TABLE 9

Quarter 5-spot tertiary recovery factor sensitivity study to capillary desaturation curve and to a pre-existent waterflood (abbreviated 'WF' in the table) of variable duration (see *Fig. 5*)

	CDC	'Infinite' WF	1.5 PV WF	1.0 PV WF	0.5 PV WF
Recovery factor (% OOIP)	[1]	8%	20%	23%	29%
Relative variation (from the 'infinite' WF case)	[1]	–	+150%	+188%	+263%
Recovery factor (% OOIP)	[6]	28%	35%	38%	44%
Relative variation (from the 'infinite' WF case)	[6]	–	+25%	+36%	+57%

N_c-shift of the CDC results in mutliplying the recovery factor by 1.75.

Next, we investigate the 'benefit' of a secondary pre-existing waterflood of variable duration on the tertiary oil recovery expressed in % OOIP in the case of the two extreme CDCs [1] and [6], which are reported in Figure 5d. In that case, the tertiary injection schedule reported in Table 8 is completed with a waterflood of three durations: 0.5, 1.0 and 1.5 injected PV. The corresponding full recoveries are reported in Figure 5e. The 0.5, 1.0 and 1.5 PV waterfloods respectively lead to a quite realistic water-cut of 90, 95 and 98%, independently of the CDC. While the CDC [1] leads to a 55% OOIP final recovery, the CDC [6] leads to a 75% OOIP final recovery; these recoveries seem far from being unlikely or unrealistic.

Finally, we 'separate' in each flood the waterflood oil recovery contribution from the one due to the chemical flood. To do so, we redefine in each flood (three floods for CDC [1] and three floods for CDC [6]) the time origin as the end of the waterflooding, that is 0.5, 1.0 and 1.5 injected PV respectively and we reset accordingly the oil recoveries. Tertiary recovery factors are reported in Figure 5f, and should be compared with the ones reported in Figure 5c, where the waterflood is supposed to be of infinite duration and therefeore has not been simulated (*i.e.* no mobile oil is left by waterflooding). While CDC [1] leads in the case of a perfect tertiary displacement to a 8% OOIP recovery factor, it leads respectively to a 29, 23 and 20% OOIP recovery factor with a pre-existing waterflood of 0.5, 1.0 and 1.5 injected PV duration. While CDC [6] leads in the case of a perfect tertiary displacement to a 28% OOIP recovery factor, it leads respectively to a 44, 38 and 35% OOIP recovery factor with a pre-existing waterflood of 0.5, 1.0 and 1.5 injected PV duration. Table 9 summarizes these results.

CONCLUSIONS

The following conclusions are drawn:

- the fundamental mechanisms for tertiary displacement of oil by surfactant enhanced alkaline and polymer flooding are successfully introduced in a C-EOR reservoir simulator (C-EOR stands for chemical EOR);
- good agreement is obtained between coreflood experiments using alkaline/surfactant/polymer chemicals to recover residual oil and our chemical simulator;
- various options as ion exchange with precipitation/dissolution and a pseudo-representation of alkali propagation are validated with dedicated experiments;
- sensitivity studies show the drastic effect of adsorption on oil recovery which has a crucial impact on C-EOR economics;
- scaling to pilot size is determinant to demonstrate the efficiency of C-EOR. This can be done using SARIP^{CH} with physical data fully validated at core scale.

REFERENCES

1 Moreau P., Morvan M., Rivoal P., Bazin B., Douarche F., Argillier J.-F., Tabary R. (2010) An integrated workflow for chemical EOR pilot design, *SPE Improved Oil Recovery Symposium*, Tulsa, Oklahoma, 24-28 April, *SPE Paper* 129865.

2 Bazin B., Yang C.Z., Wang D.C., Su X.Y. (1992) Micellar flooding in an alkaline environment under Lao Jun Miao conditions, *International Meeting on Petroleum Engineering*, Beijing, China, 24-27 March, *SPE Paper* 22363.

3 Martin F.D., Oxley J.C. (1985) Effect of various alkaline chemicals on phase behavior of surfactant/brine/oil mixtures, *SPE Oilfield and Geothermal Chemistry Symposium*, Phoenix, Arizona, 9-11 March, *SPE Paper* 13575.

4 Nelson R.C., Lawson J.B., Thigpen D.R., Stegemeier G.L. (1984) Cosurfactant-enhanced alkaline flooding, *SPE Enhanced Oil Recovery Symposium*, Tulsa, Oklahoma, 15-18 April, *SPE Paper* 12672.

5 Beicip-Franlab, see www.beicip.com/index.php/eng/software/reservoir/simulation/pumaflow

6 Standing M.B. (1975) *Notes on relative permeability relationships*, Lecture Notes, Trondheim, Norway.

7 Moore T.F., Slobod R.L. (1956) The effect of viscosity and capillarity on the displacement of oil by water, *Producers Monthly* **20**, 10, 20-30.

8 Taber J.J. (1969) Dynamic and static forces required to remove a discontinuous oil phase from porous media containing both oil and water, *SPE Paper* 2098, *SPE J.* **9**, 3-12.

9 Stegemeier G.L. (1974) Relationship of trapped oil saturation to petrophysical properties of porous media, *SPE Improved Oil Recovery Symposium*, Tulsa, Oklahoma, 22-24 April, *SPE Paper* 4754.

10 Stegemeier G.L. (1977) Mechanisms of entrapment and mobilization of oil in porous media, in: Shah D.O., Schechter R.S. (eds), Improved oil recovery by surfactant and polymer flooding, Academic Press, pp. 55-91.

11 Lake L.W. (1989) *Enhanced oil recovery*, Prentice-Hall.

12 Abrams A. (1975) The influence of fluid viscosity, interfacial tension and flow velocity on residual oil saturation left by waterflood, *SPE Paper* 5050, *SPE J.* **15**, 5, 437-447.

13 Taber J.J. (1981) Research on enhanced oil recovery: past, present and future, in *Surface phenomena in enhanced oil recovery*, Shah D.O. (ed.), Plenum Press, pp. 13-52.

14 Delshad M. (1990) Trapping of micellar fluids in Berea sandstone, *PhD Thesis*, The University of Texas at Austin.

15 Shah D.O., Schechter R.S. (eds) (1977) *Improved oil recovery by surfactant and polymer flooding*, Academic Press.

16 Shah D.O. (ed.) (1981) *Surface phenomena in enhanced oil recovery*, Plenum Press.

17 Souto E., Bazin B., Sardin M. (1993) Ion exchange between hydrogen and homoionic brines related to permeability reduction, *SPE International Symposium on Oilfield Chemistry*, New Orleans, Louisiana, 2-5 March, *SPE Paper* 25203.

18 Labrid J.C., Le Thiez P., Minssieux L. (1992) A numerical model for predicting alkali slug migration in chemical processes, *SPE/DOE Enhanced Oil Recovery Symposium*, Tulsa, Oklahoma, 22-24 April, *SPE Paper* 24189.

19 Bazin B., Labrid J. (1991) Ion exchange and dissolution/precipitation modeling: application to the injection of aqueous fluids into a reservoir sandstone, *SPE Paper* 18464, *SPE Resew. Eng.* **6**, 2, 233-238.

20 Mohammadi H., Delshad M., Pope G.A. (2008) Mechanistic modelling of alkaline/surfactant/polymer floods, *SPE/DOE Symposium on Improved Oil Recovery*, Tulsa, Oklahoma, 20-23 April, *SPE Paper* 110212.

21 Flaaten A.K., Nguyen Q.P., Zhang J., Mohammadi H., Pope G.A. (2008) ASP chemical flooding without the need for soft water, *SPE Annual Technical Conference and Exhibition*, Denver, Colorado, 21-24 Sept., *SPE Paper* 116754.

22 Huh C. (1979) Interfacial tensions and solubilizing ability of a microemulsion phase that coexists with oil and brine, *J. Colloid Interface Sci.* **71**, 2, 408-426.

23 Willhite G.P. (1986) *Waterflooding*, SPE Textbook Series Vol. 3, Society of Petroleum Engineers.

Final manuscript received in June 2012
Published online in January 2013